Astronomy & Astrophysics manuscript no. gpspaper
June 23, 2008

© ESO 2008

arXiv:0806.3694v1 [astro-ph] 23 Jun 2008

Quasi-simultaneous multi-frequency observations of inverted-spectrum GPS candidate sources *

B. Vollmer[1], T.P. Krichbaum[2], E. Angelakis[2], Y.Y. Kovalev[2,3]

[1] CDS, Observatoire astronomique de Strasbourg, 11, rue de l'université, 67000 Strasbourg, France
[2] Max-Planck-Insitut für Radioastronomie, Auf dem Hügel 69, 53121 Bonn, Germany
[3] Astro Space Center of Lebedev Physical Institute, Profsoyuznaya 84/32, 117997 Moscow, Russia

Received / Accepted

ABSTRACT

Context. Gigahertz-Peaked Spectrum (GPS) sources are probably the precursors of local radio galaxies. Existing GPS source samples are small (< 200).
Aims. It is necessary to extend the availabe sample of the Gigahertz-Peaked Spectrum (GPS) and High Frequency Peaker (HFP) sources in order to study their nature with greater details and higher statistical significance.
Methods. A sample of 214 radio sources, which were extracted from the SPECFIND catalog and show an inverted radio spectrum, were observed quasi-simultaneously at 4.85, 10.45, and 32 GHz with the 100-m Effelsberg radio telescope. Using the VLBA calibrator survey (VCS) we have investigated the parsec-scale morphology of the sources.
Results. About 45% of the sources in our sample are classified as GPS or HFP candidates. We add 65 new GPS/HFP candidates to existing samples. We confirm the expected tendency that HFP are more compact on milliarcsecond scale than the 'classical' GPS sources, which peak at lower frequencies.
Conclusions. The data mining of the SPECFIND database represents a promising tool for the discovery of new GPS/HFP sources.

Key words. radio continuum: galaxies — galaxies: active

1. Introduction

GHz-Peaked Spectrum (GPS) sources are powerful ($\log P_{1.4\ \mathrm{GHz}} > 25\ \mathrm{W\,Hz^{-1}}$) and compact ($< 1$ kpc) extragalactic radio sources, which show a convex radio spectrum peaking between 500 MHz and 10 GHz in the observer's frame (for a review see O'Dea 1998). The physical mechanism responsible for the turnover of the spectrum is still unclear with two competing models proposed: the synchrotron self-absorption caused by dense plasma within the source or the free-free absorption caused by a screen external to the source.

High Frquency Peakers (HFP) are radio sources defined via their convex spectrum peaking at frequencies above 5 GHz (Dallacasa et al. 2000). From the anti-correlation found between the turnover frequency and size (O'Dea & Baum 1997) HFPs are expected to be smaller and therefore younger radio sources than GPS sources.

GPS sources are associated with either quasars or galaxies. Despite the similar shape of their radio spectrum, these two classes of GPS sources are often considered to be different. Torniainen et al. (2005), who studied the long term variability of 35 inverted-spectrum sources, concluded that genuine quasar-type GPS sources are rare. They found a large number of highly variable blazar sources that can have a convex spectrum peaking at high frequencies (up to $\sim$100 GHz) during flaring events occurring in the radio jets.

The nature of GPS sources is still under debate. Two possible scenarios have been put forth: (i) the 'frustration' scenario, according to which the small size and the inverted spectrum are caused by a dense environment that prohibits the source from growing larger (e.g., Gopal-Krishna & Wiita 1991), (ii) the 'youth' scenario, suggesting that the GPS sources represent the young precursors of compact steep spectrum (CSS) sources and extended radio sources (e.g., Mutel & Phillips 1988, Fanti et al. 1990, 1995).

There is now a wide consensus that, at least the symmetric GPS sources, represent the early evolutionary stage of the extended radio source population. At this stage the radio emitting region grows and expands within the interstellar medium before plunging into the intergalactic medium to form an FR II radio source (Fanti et al. 1995, Readhead et al. 1996, Begelman 1996, Snellen et al. 2000a).

The detection of kpc-scale emission associated with a few GPS sources seems to be inconsistent with a recent origin of the radio activity. Such an extended emission is interpreted as a sign of a past nuclear activity. In this case the GPS source, i.e. the galactic nucleus, is at the beginning of a new cycle of activity. Since extended radio emission around GPS sources is a rare phenomenon, Stanghellini et al. (2005) conclude that the time scale between subsequent phases of activity is in general longer than the radiative lifetime of the radio emission from the earlier activity ($\sim 10^8$ yr).

Send offprint requests to: B. Vollmer: bvollmer@astro.u-strasbg.fr

[*] Tables 5 and 6 are only available in electronic form at the CDS via anonymous ftp to cdsarc.u-strasbg.fr (130.79.128.5) or via http://cdsweb.u-strasbg.fr/cgi-bin/qcat?J/A+A/.

The currently existing GPS sample is limited (< 200 objects, see, e.g., the recent compilation by Labiano et al. 2007). In order to conduct statistical studies of GPS objects and test whether the number of GPS sources at intermediate redshifts is in accordance with that of local FR II radio galaxies, it is necessary that the sample of available GPS sources is extended. In particular, this could help to test whether GPS sources are the precursors of the local FR II radio galaxies.

In this paper, we present results of a search for new GPS/HFP candidates. Since the identification of a radio source as a genuine young GPS source depends on the detailed knowledge of its spectrum, flux density variability, VLBI structure and source identification, we will use in the following the words GPS or HFP source as a synonym for GPS candidate or HFP candidate. In order to measure radio-spectra over a range of high frequencies, which are not affected by non-contemporanous measurements, we observed a sample of 214 objects north of declination −25° that show an inverted radio spectrum, with quasi-simultaneous flux density measurements at 4.85 GHz, 10.45 GHz, and 32 GHz using the Effelsberg 100-m telescope of the Max-Planck-Institut für Radioastronomie (MPIfR). In Sect. 2 we review the sample selection procedure implemented on the basis of the SPECFIND database, observations and primary data reduction are described in Sect. 3. We present results of observations in Sect. 4, sources extention and variablility characteristics in Sect. 5, cross-identification and spectral fitting in Sect. 6, milliarcsecond-scale compactness and morphology in Sect. 7, comparison with other available GPS/HFP samples in Sect. 8. We summarize our results in Sect. 9.

2. Sample selection

SPECFIND (Vollmer et al. 2005a) is a hierarchical algorithm. It classifies a source j as parent, sibling, or child with respect to a given source i using a procedure which has different stages:
stage 1: cross-identification based on proximity criteria taking into account the resolution and source size,
stage 2: cross-identification based on flux densities at the same frequency,
stage 3: cross-identification based on flux density at different frequencies, as expected from the radio spectral index, adopting the convention $S_\nu \propto \nu^\alpha$.

At the end of this procedure a source i and its siblings are considered to be the same source. If source j is identified as a parent, source i might be a resolved sub-source of source j. If source i has children, it might be extended, and the children represent its resolved sub-sources. At the end of the cross-identification the self-consistency of the hierarchy and the uniqueness is tested. A radio source cannot be assigned to more than one physical object. The position of each object is taken from the radio source observed with the highest resolution (for the positional accuracy of the included radio surveys see Vollmer et al. 2005b).

The result of the cross-identification depends strongly on the detailed spectrum fitting algorithm (Vollmer et al. 2005a), the initial set of frequency points and their weights. During this procedure non-fitted frequency points are rejected and removed from the spectrum, since they may belong to a different object. SPECFIND determines the slope and the abscissa for a given source i with all other cross-identified sources. It is required that the final power law fits source i within the errors. Therefore, the result of the fitting algorithm can be different depending on the choice of source i. A given object with an associated radio spectrum can thus possess several slopes and abscissa.

From an extended version of the SPECFIND catalog[1], which contains the comparison samples described in table 5 of Vollmer et al. (2005a), we extracted objects with a maximum slope (spectral index, α) greater or equal 0.5 and declination $\delta > -25°$. The frequency range in which the spectral index is determined depends on the actual frequency coverage and sensitivity of the 22 individual radio catalogues used by SPECFIND. To avoid confusion problems for the flux density measurements performed at Effelsberg, we then removed all sources which are extended in the NVSS (larger than the 45" beam size; Condon et al. 1998) and some galactic sources, which coincide with known HII regions.

This resulted in a list of 214 objects. The majority of the sources has a spectral index of around +0.5. The distribution of spectral indices of these sources is shown in Fig. 1, and their distribution on the sky is shown in Fig. 2. About one third of them (69) are located within ±10° from the Galactic plane. Some of them were later identified as infrared sources or planetary nebula. Since our selection criterion is only based on the shape of the radio spectrum, we did not remove these sources. The number of targets is smaller in the southern hemisphere than in the northern hemisphere because of the lack of deep surveys in the southern hemisphere (Vollmer et al. 2005a).

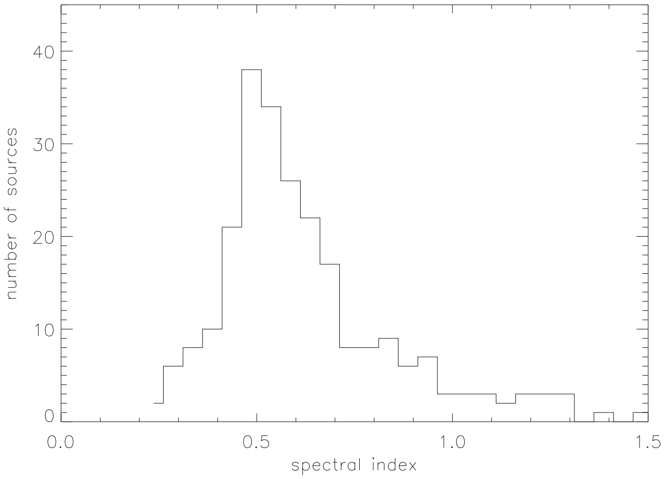

Fig. 1. SPECFIND spectral index distribution of the sources in our sample. The power law spectrum is defined by $S_\nu \propto \nu^\alpha$. All the objects have several spectral indices depending on the weighting of the frequency points. Objects with $\alpha < 0.5$ have at least one associated spectral index ≥ 0.5.

3. Observations and primary data reduction

The flux density measurements of the 214 target sources were made with the 100-m MPIfR radio telescope in

---

[1] available at CDS VizieR (Ochsenbein et al. 2000)

Table 1. Effelsberg observing sessions

Date	UT range (hr)
23, 24 Sep 2005	11–08
8, 9 Oct 2005	07–04
17, 18 Jan 2006	18–02
24, 25 Jan 2006	16–08
30, 31 Jan 2006	15–08
24 Mar 2006	02–10

Effelsberg (Germany). The observations took place in 6 observing sessions which are summarized in Table 1.

In each session the target sources and the calibrator sources (see Table 2) were observed with the heterodyne receivers mounted on the secondary focus of the telescope. The measurements were made at 6 cm (4.85 GHz), 2.8 cm (10.45 GHz) and 9 mm (32 GHz). The receiver characteristics are summarized in Table 3. Column 1 gives the observing wavelength, column 2 the central frequency, column 3 the observing bandwidth, column 4 the typical system temperature (at zenith), column 5 the typical peak value of the elevation-dependent antenna gain, column 6 the size of the observing beam (full width at half maximum, FWHM), column 7 the polarization of the receiver feeds, column 8 the number of receiver horns used in the data reduction[2], and column 9 the receiver type. The signal from the second receiver horn allowed the off-source signal containing the (time variable) atmospheric signal to be subtracted from the signal on the source (beam switch). This improved the data quality and led to almost flat baselines in each scan.

For each source, the antenna temperature was measured using the method of 'cross-scans'. Here, the telescope beam is repeatedly moved across the source position, with an equal number of sub-scans in elevation and in azimuth direction. The number of sub-scans in each cross-scan ranged between $4-12$, depending on the flux density of the source and the stability of the telescope pointing. Each source was measured with at least two cross-scans at each of the three observing bands. With a typical duration of 25-30 seconds for each sub-scan and scan lengths of $600''$, $220''$, and $110''$ at $\lambda = 6$ cm, 2.8 cm, & 9 mm, respectively, each scan lasted between $3-5$ min. This allowed us to obtain for each source 'quasi-simultaneous' flux density measurements at the 3 observing bands within a $15-20$ min time interval.

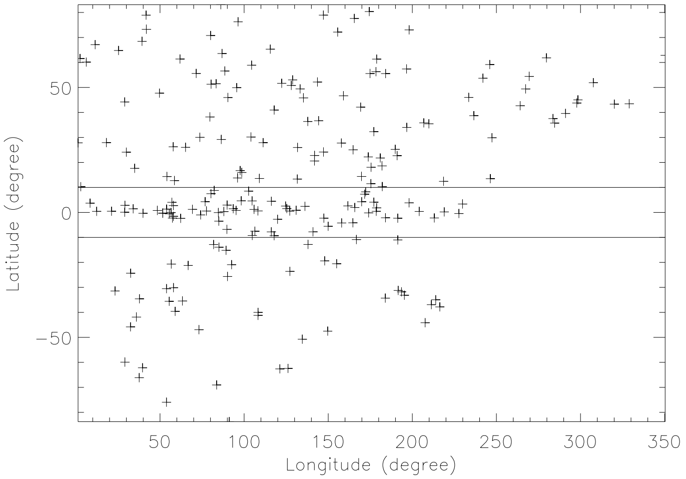

Fig. 2. Spatial distribution of our sample of 214 sources with an inverted radio spectrum in Galactic coordinates . The horizontal lines mark galactic latitudes of ±10°.

Table 2. The primary and the secondary calibrators along with and their flux densities at the observing frequencies.

Source	$S_{6\mathrm{cm}}$ [Jy]	$S_{2.8\mathrm{cm}}$ [Jy]	$S_{9\mathrm{mm}}$ [Jy]	Comment
3C48	5.48	2.60	0.80	Primary Calibrator
3C138	3.79	2.16	0.92	Secondary Calibrator
3C147	7.90	3.82	1.18	Secondary Calibrator
3C161	6.62	3.06	0.83	Secondary Calibrator
3C286	7.48	4.45	1.82	Primary Calibrator
3C295	6.56	2.62	0.55	Primary Calibrator
NGC7027	5.48	5.92	5.49	Primary Calibrator

After the observations, the data were reduced in the standard manner following the procedures described in Kraus et al. (2003). To derive the flux densities of the observed point sources, Gaussian profiles were fitted to each sub-scan in each driving direction. For fainter sources, the sub-scans were averaged in each driving direction before the Gaussian fitting was done. After correcting for small residual pointing offsets, the amplitudes of the individual sub-scans were combined by averaging them. For each scan and source this resulted in the uncalibrated antenna temperature as determined by the peak value, S^{peak}, of the Gaussian fit. For each scan, also the half-power beam width, $HPBW^{\mathrm{obs}}$, was measured. In the next step we corrected the measurements for the elevation-dependent antenna gain and for systematic time-dependent effects, using standard gain-elevation curves and the known flux densities of the primary and secondary calibrators, which where observed regularly at $3-6$ hr intervals throughout each of the observing sessions. Opacity corrections were applied to the 9 mm data. The conversion from antenna temperature (measured in K) to flux density (measured in Jy) was done using the flux density scale of Ott et al. (1994), refined by more recent measurements (A. Kraus, priv. comm.). Table 2 summarizes the flux density scale used throughout this paper.

4. Results

The observed radio flux densities at 4.85, 10.45, and 32 GHz are listed in Table 5 along with the spectral indices between 4.85-10.45 GHz and 10.45-32 GHz. The last column of the table lists the observing frequency in GHz, at which the FWHM of the Gaussian fitted to the telescope response was significantly larger than that to the point source (see Table 3). This is indicative of extended source structure or confusion. The sources marked in this way should be regarded either as partially resolved or as being confusing within the Effelsberg observing beam. We detected all 214 sources at 4.85 GHz, 209 (98 %) sources at 10.45 GHz, and 181 (85 %) sources at 32 GHz. For the non-detected sources we assign a dash ('−') in the corresponding column of Table 5. Depending on the on-source integration time, receiver properties and weather conditions the estimated detection limits are $3\sigma = 1-5$ mJy at 4.85 GHz, $3-10$ mJy at 10.45 GHz and $10-30$ mJy at 32 GHz, with the higher numbers of each range reflecting non-optimal

---

[2] the 6-cm receiver has 2 feeds, the 2.8-cm one has 4 and the 9 mm receiver has 6 feeds

Table 3. The characteristics of the used receivers.

λ [cm]	Center ν [GHz]	Bandwidth [MHz]	T_{sys} [K]	Gain [K/Jy]	FWHM ["]	Polarization	Horns	Comment
6	4.85	500	27	1.5	146	dual circ.	2	Software Beam switch
2.8	10.45	300	50	1.3	67	dual circ.	2	Software Beam switch
0.9	32.00	2000	77	0.5	26	LCP	2	Correlation Receiver

weather conditions. The provided errors of the flux density measurements are 1σ errors and result from formal error propagation through the following steps: Gaussian fitting, gain and time correction, K/Jy conversion. The error of the absolute flux density scale (Baars et al. 1977, Ott et al. 1994) is not included in the provided errors. The error of the spectral indices follows from the Gaussian error propagation of the flux density errors.

The derived distributions of the spectral indices are shown in Fig. 3. The number of sources with a negative spectral index between 4.85 and 10.45 GHz is 142, that of sources with a negative spectral index between 10.45 GHz and 32 GHz is 139. The number of sources with a positive spectral index between 4.85 and 10.45 GHz is 67 (31 %), whereas 41 sources show a positive spectral index between 10.45 GHz and 32 GHz. Thus, $\sim 20\%$ of the sources of our sample show an inverted spectrum up to 32 GHz. Out of 214 sources 63 (29 %) are resolved by the Effelsberg beam at one or more observing frequencies. Out of the 63 resolved objects 30 are within 10° from the Galactic plane. Identification statistics about the object types are given in Sect. 8.

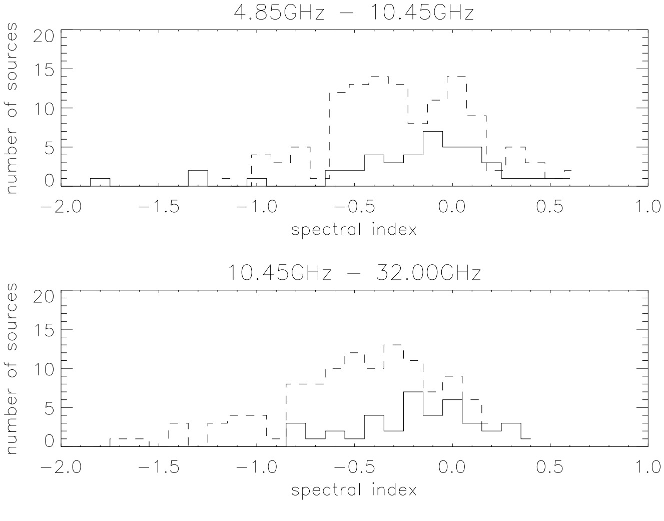

Fig. 3. The spectral index distribution for variable (solid line) and non-variable (dashed line) sources. The spectral indices have been calculated from flux densities at 4.85 GHz and 10.45 GHz (upper panel) and at 10.45 GHz and 32.00 GHz (lower panel).

5. Extended sources and variability

The source spectra extracted with SPECFIND from the database result from non-simultaneous multi-epoch flux density measurements with different telescopes. The observations described here, however, have been obtained with the 100-m Effelsberg telescope, providing for each source quasi-simultaneous measurements within 15-20 min at 3 different frequencies. One expects that radio sources with flat or inverted spectra show higher degree of variability than those with steeper spectra. In order to test this idea, we compared the Effelsberg 4.85 GHz (6 cm) flux density to a corresponding 4.85 GHz flux density in SPECFIND whenever that is available (121 sources of our sample). The SPECFIND used 4.85 GHz flux densities obtained with angular resolutions of $3.5'$and $2.8'$ (Gregory et al. 1996; Gregory & Condon 1991; Becker et al. 1991; Wright et al. 1994, 1996; Griffith et al. 1994, 1995; Bennett et al. 1986; Langston et al. 1990, Griffith et al. 1990, 1991), compared to the Effelsberg 100-m telescope resolution of $2.4'$. Therefore, extended or confusing sources observed with these different beam sizes can also lead to differences between the Effelsberg and the SPECFIND fluxes.

Since the SPECFIND catalog may contain more than one flux density at 4.85 GHz, we base our variability/confusion criterion on the maximum of the absolute value of the differences between the SPECFIND and the Effelsberg 4.85 GHz flux densities $\Delta S_{4.85\ \mathrm{GHz}} = S^{\mathrm{Eff}}_{4.85\ \mathrm{GHz}} - S^{\mathrm{SPECFIND}}_{4.85\ \mathrm{GHz}}$:

$$\max(|\Delta S_{4.85\ \mathrm{GHz}}|)/S^{\mathrm{Eff}}_{4.85\ \mathrm{GHz}} \geq 0.5\ , \qquad (1)$$

where $S^{\mathrm{Eff}}_{4.85\ \mathrm{GHz}}$ is the Effelsberg and $S^{\mathrm{SPECFIND}}_{4.85\ \mathrm{GHz}}$ is the SPECFIND flux density at 4.85 GHz. In addition, we require no overlap between the SPECFIND and Effelsberg 4.85 GHz points within the errors. After applying this criterion we find that 59 out of 197 sources are suspected to be variable or confusing. This represents 30% of the restricted sample (197 sources having a SPECFIND frequency point at 4.85 GHz) and 28% of the whole sample (214 sources). Based on these numbers we expect about 30% of the sources in our sample to be variable at centimeter wavelengths. Out of the identified 59 variable sources 10 are quasars, 4 are BL Lacertae object, 3 are galaxies, 3 are X-ray sources, 4 are infrared sources, and 1 is a planetary nebula (PN). As expected, the variable sources tend to be either BL Lacs or quasars (see also Tornianinen et al. 2005).

The information about the source extension and variability can be found in column 7 of Table 6. There, the apparently variable/confusing sources based on the 4.85 GHz flux densities are marked with the symbol 'V'. The letter 'E' indicates sources whose extensions are larger than the beam of the Effelsberg telescope at at least one frequency. We find 30 variable sources which are extended or confusing in at least one of our Effelsberg observations (designated as 'EV'). Fig. 3 shows the spectral index distribution for variable and non-variable sources. Variable sources have in general a flatter spectral index between 4.85 – 10.45 GHz and 10.45 – 32 GHz. We did not test for variability at 10.45 GHz and 32 GHz, because there are not many measurements available in the database at these frequencies to compare with.

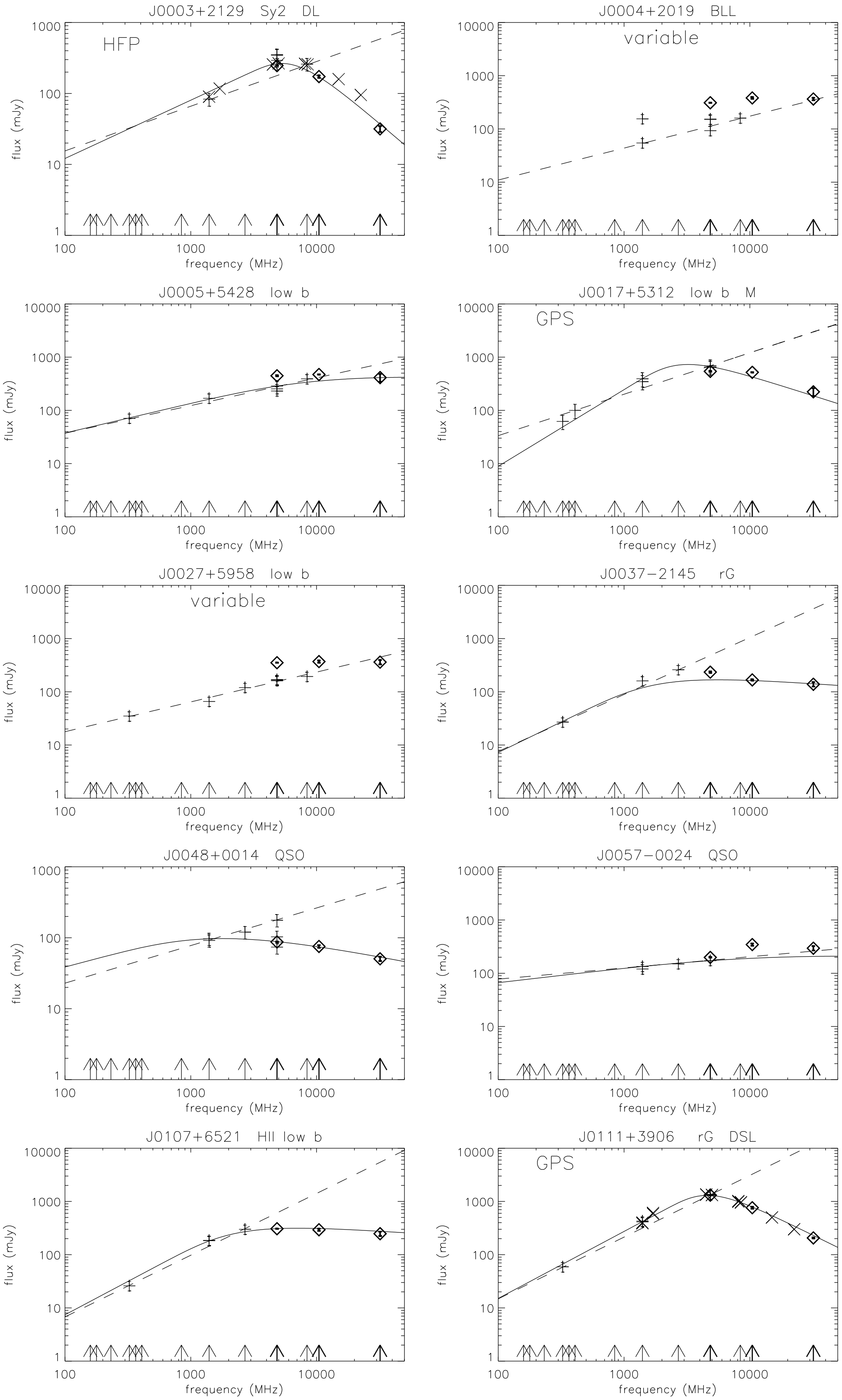

Fig. 4. Radio spectra. SPECFIND data are plotted as pluses with associated error bars, the Effelsberg flux densities as diamonds, and the flux densities obtained by Dallacasa et al. (2000) as crosses. Dashed line: power law fitted by SPECFIND; solid line: fitted spectrum (Eq. 2). GPS: GHz-Peaked Spectrum; HFP: High Frequency Peaker. On top of each panel the source name, object type (if available), and membership of an existing sample (Table 4) are given. A source located ±10° from the Galactic plane is labeled with “low b”. The arrows on the frequency axis indicate the frequencies of the radio catalogs included in SPECFIND (Vollmer et al. 2005a). *The full figure is available in the online version of the Journal.*

6. Cross-identification and GPS spectrum fitting

Fig. 4 shows the combined radio spectra from our Effelsberg observations (diamonds) and the SPECFIND catalog (plus signs with error bars) along with the SPECFIND power law spectrum (dashed line). We cross-identified our sources with the CDS SIMBAD database (Wenger et al. 2000). The obtained object types are indicated at the top of each panel and in Table 6. We have cross-identified 108 objects: 45 quasars, 7 Seyfert or LINER galaxies, 8 BL Lacs, 15 galaxies, 8 X-ray sources, 8 infrared sources, 8 planetary nebulae, 2 stars, and 2 HII regions. Additionally, we added 5 quasar identifications from Véron & Véron (2006). As one can see in this list, there are 12 confirmed Galactic sources. As expected, young planetary nebulae and compact HII regions can also show an inverted radio spectrum up to the GHz regime. In addition, the infrared sources located at ±10° from the Galactic plane, which are all extended, are most probably also of Galactic nature. We end up with 80 confirmed extragalactic sources with 60% of them being quasars (from SIMBAD and Véron & Véron 2006).

Following Snellen et al. (1998) the combined radio spectra were fitted by the function:

$$S(\nu) = \frac{S_{\max}}{1-\mathrm{e}^{-1}} \times \left(\frac{\nu}{\nu_{\max}}\right)^{k} \times \left(1-\mathrm{e}^{-(\frac{\nu}{\nu_{\max}})^{l-k}}\right) , \qquad (2)$$

where k is the optically thick spectral index, l the optically thin spectral index, and $S_{\max}$ and $\nu_{\max}$ respectively the peak flux density and peak frequency. The optically thick spectral index k was set to the SPECFIND spectral index (slope of the dashed line in Fig. 4) or to the spectral index between the two points with the lowest frequencies, if this allowed a better fit. For the optically thin spectral index, we used the spectral index between the two points at the highest frequencies available. The peak flux density and peak frequency were then determined with a least square fit method. We also determine the FWHM and $\Delta = \log(FWHM\ (\mathrm{MHz}))$ of the fitted function (Eq. 2). A radio source is defined as a GPS if $0 < \Delta \leq 2.5$ and $\nu_{\max} \leq 5$ GHz. Following Dallacasa et al. (2000) sources with $0 < \Delta \leq 2.5$ and $\nu_{\max} > 5$ GHz or sources with $\alpha > 0.5$ between 1.4 and 5 GHz and $\alpha > 0$ between 10 and 32 GHz are classified as High Frequency Peakers (HFP). With these definitions we find 38 GPS and 53 HFP sources. The fitted peak or turnover frequencies can be found in column 8 of Table 6. The distribution of peak flux densities is shown in Fig. 5. Most of our sources have a peak flux density around 0.2 Jy. Our GPS/HFP candidate source sample (Table 6) comprises 18 extended/confusing sources and 4 variable sources (Eq. 1). These objects are likely blazars rather than genuine young GPS/HFP sources.

7. Milliarcsecond-scale properties

To investigate parsec-scale characteristics of the sample, we have measured the VLBI compactness at 2.3 and 8.6 GHz as described in Kovalev et al. (2005) using the VLBA[3] Calibrator Survey (VCS, Beasley et al. 2002, Fomalont et al. 2003, Petrov et al. 2005, 2006, 2008, Kovalev et al. 2007). The compactness is defined as the ratio of the correlated flux density measured at long interferometer spacings (*uv*-spacings) and the integrated flux density from a VLBI image. Typical errors of the compactness determination are about 0.05. The error can rise up to 0.1 for the sources with integrated flux density about or less than 0.1 Jy.

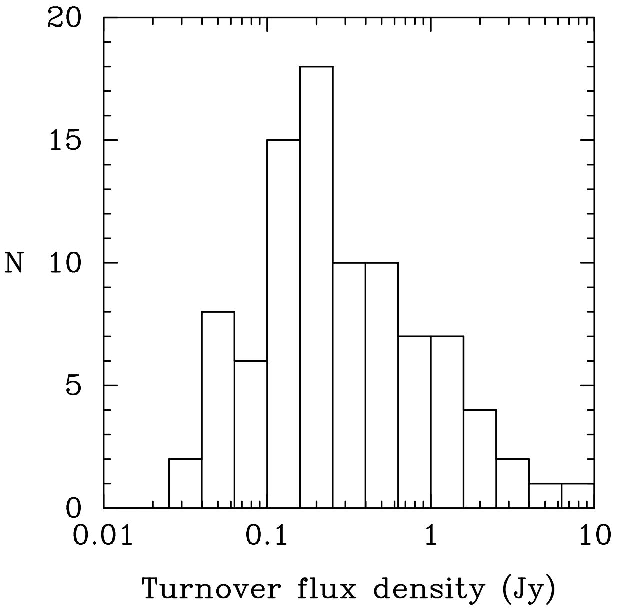

Fig. 5. Distribution of peak flux densities of GPS sources from Table 6.

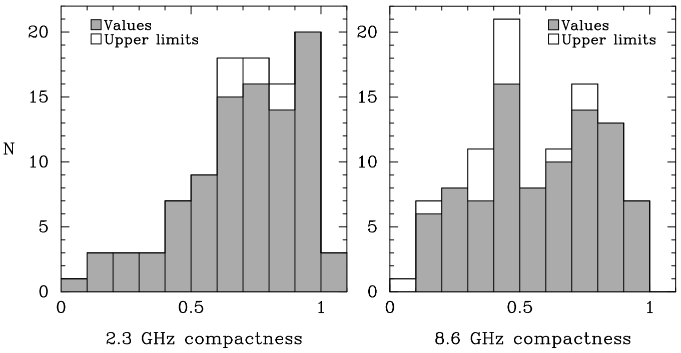

Fig. 6. VLBI compactness ratios at 2.3 GHz (left panel) and 8.6 GHz (right panel).

Our sample contains 108 sources from the VLBA Calibrator Survey (Table 6 and Fig. 6). For further analysis it is convenient to discriminate between almost point-like and partially resolved sources. We define a source as (almost) point-like if its compactness is larger than 0.7. Whereas more than half of the sources are compact at 2.3 GHz, the distribution of the compactness at 8.6 GHz is approximately flat (Fig. 6).

The majority of HFP candidate sources (21 out of 35) appear point-like at 2.3 GHz whereas 14 out of 21 GPS candidate sources are extended at this frequency. Genuine GPS/HFP candidate sources are expected to be resolved at both frequencies with compactness values decreasing with increasing frequency. We find that 24 out of 53 GPS/HFP candidate sources with available compactness information do show this behavior. Indeed the median compactness values are 0.55 (GPS) and 0.75 (HFP) at 2.3 GHz, while at 8.6 GHz they decrease to 0.37 (GPS) and 0.44 (HFP).

---

[3] Very Long Baseline Array of the National Radio Astronomy Observatory

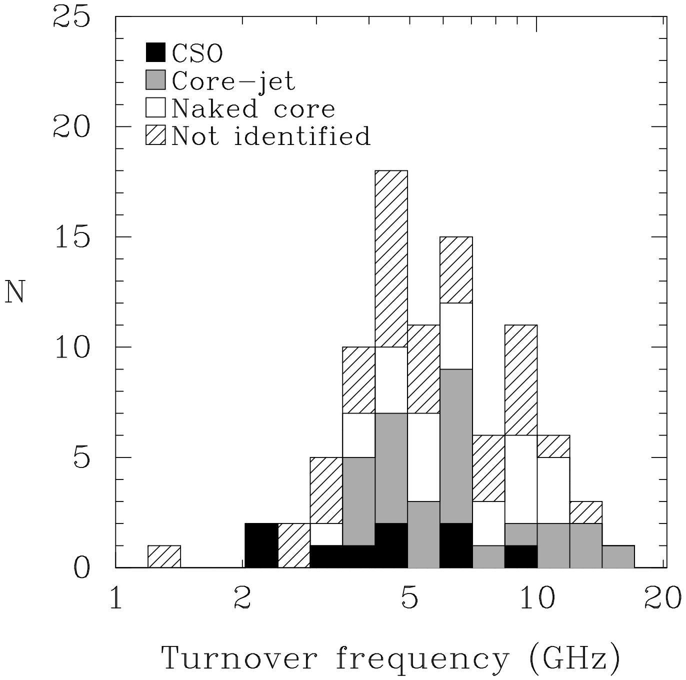

Fig. 7. The distribution of the turnover frequencies for the different VLBI morphology classes.

In a second step, we classified the sources based on their morphology in the two-frequency VLBI images. This classification is summarized in column 13 of Table 6: 'nc'—naked core candidate; 'cj'—core jet candidate; 'cso'—compact symmetric object candidate. A source is classified here as a cso if distinct components of its dual-frequency VLBA structure have 2.3–8.6 GHz spectral index values which differ by less than 0.5. It is important to note that, on the basis of the two-frequency VLBI data alone, one cannot definitely decide whether an object is a classical compact symmetric one. Rather a multi-band VLBI study is needed in order to reach a definite conclusion (e.g., Peck & Taylor 2000, Snellen et al. 2000b, Xiang et al. 2002, 2005, 2006, Orienti et al. 2006). A "deeper" VLBI experiment could also detect a weak jet in many sources classified here as naked cores. In summary, we identify 65 previously unknown GPS/HFP candidate sources out of which 32 are listed also in the VLBA Calibrator survey catalog.

In Fig. 7 we show the distribution of the turnover frequencies for the different VLBI morphology classes. Most of the sources are point-like (naked cores), about half of this number have additional jets detected and 9 sources are classified as compact symmetric object candidates. The CSO candidates which are extended at the milliarcsecond-scale, tend to have lower values of the turnover frequency in comparison to the properties of the full sample.

8. Comparison with other GPS/HFP samples

In order to investigate if our objects are already identified as GPS/HFP sources, we cross-identified our sample with existing GPS/HFP samples of Snellen et al. (1998), Stanghellini et al. (1998), Marecki et al. (1999), Dallacasa et al. (2000), Fanti et al. (2001) and Labiano et al. (2007). Table 4 shows the results of this cross-identification. The sample designations can also be found in column 6 of Table 6 and on top of each plot in Fig. 4. We find 32 previously known GPS/HFP sources in our sample, out of which 26 are classified as GPS/HFP candidates by us. Dallacasa et al. (2000) made quasi-simultaneous multi-frequency observations of HFP sources at the VLA. We have plotted their flux densities as crosses on the spectra of Fig. 4. For the majority of the sources there is a good agreement with the Effelsberg and SPECFIND flux densities.

Table 4. Cross-identification with existing GPS/HFP samples.

Article	Designation	Number of objects
Snellen et al. (1998)	B	3
Stanghellini et al. (1998)	S	7
Fanti et al. (2001)	F	0
Dallacasa et al. (2000)	D	15
Marecki et al. (1999)	M	9
Labiano et al. (2007)	L	14

9. Summary

A sample of 214 radio sources with inverted spectra and declination $\delta > -25°$ was extracted from the SPECFIND catalog (Vollmer et al. 2005a). This catalog contains cross-identifications of radio sources from surveys at different frequencies and combines them into one single radio spectrum per object. To obtain quasi-simultaneous radio spectra, we observed those sources with the MPIfR Effelsberg 100-m radio telescope at 4.85, 10.45, and 32 GHz. All the observed sources were detected at 4.85 GHz, while 209 and 180 sources were detected at 10.45 GHz and 32 GHz, respectively. We expect the fraction of variable or confusing sources in our complete sample to be of $\sim 30\%$. On the basis of the performed analysis of continuum radio spectra, we have identified 38 GPS and 53 HFP candidates out of which 65 were previously unknown. An inspection of VCS data shows that 24 out of 53 GPS/HFP sources with available VCS data are resolved at 2.3 and 8.6 GHz. We have confirmed the expected tendency for HFP objects to be highly compact and the GPS ones to show a significantly lower level of compactness at the milliarcsecond scale. This independently supports robustness of our source classifications presented here.

We have a success of ∼45% for finding GPS/HFP candidates from a selected SPECFIND catalog sample. Once the SPECFIND catalog is upgraded with the inclusion of more radio catalogs, this method comprises a promising way for future identification of new GPS/HFP sources.

Acknowledgements. This work is based on observations with the 100-m telescope of the MPIfR (Max-Planck-Institut für Radioastronomie) at Effelsberg. We would like to thank A. Kraus for his help. Y. Y. Kovalev is a Research Fellow of the Alexander von Humboldt Foundation. We would like to thank John McKean for fruitful discussions. We thank the anonymous referee for thoughtful reading and useful comments which helped to improve the manuscript.

References

Baars, J.W.M., Genzel, R., Pauliny-Toth, I.I.K., Witzel, A., 1977, A&A 61, 99

Beasley, A.J., Gordon, D., Peck, A.B., et al. 2002, ApJS, 141, 13

Becker R.H., White R.L., & Edwards A.L. 1991, ApJS, 75, 1 (BWE)
Begelman, M.C. 1996, in: Cygnus A – Study of a Radio Galaxy, Proceedings of the Greenbank Workshop, edited by C.L. Carilli and D.E. Harris. Cambridge University Press, p.209
Bennett C.L., Lawrence C.R., Burke B.F., Hewitt J.N., & Mahoney J. 1986, ApJS, 61, 1 (MITG)
Condon, J.J., Cotton, W.D., Greisen, E.W., et al. 1998, AJ, 115, 1693
Dallacasa, D., Stanghellini, C., Centonza, M., Fanti, R. 2000, A&A, 363, 887
Fanti, R., Fanti, C., Schilizzi, R.T., et al. 1990, A&A, 231,333
Fanti, C., Fanti, R., Dallacasa, D., et al. 1995, A&A, 302, 317
Fanti, C., Pozzi, F., Dallacasa, D., et al. 2001, A&A, 369, 380
Fomalont, E.B., Petrov, L., MacMillan, D.S., Gordon, D., Ma, C. 2003, AJ, 126, 2562
Gopal-Krishna & Wiita, P.J. 1991, ApJ, 373, 325
Gregory P.C. & Condon J.J. 1991, ApJS, 75, 1011 (87GB)
Gregory P.C., Scott W.K., Douglas K., & Condon J.J. 1996, ApJS, 103, 427 (GB6)
Griffith M., Langston G., Heflin M. et al. 1990, ApJS, 74, 129 (MITG)
Griffith M., Heflin M., Conner S., Burke B., & Langston G.,1991, ApJS, 75, 801 (MITG)
Griffith M.R., Wright A.E., Burke B.F., & Ekers R.D. 1994, ApJS, 90, 179 (PMNT)
Griffith M.R., Wright A.E., Burke B.F., & Ekers R.D. 1995, ApJS, 97, 347 (PMNE)
Kovalev, Y.Y., Kellermann, K.I., Lister, M.L., et al. 2005, AJ, 130, 2473
Kovalev, Y.Y., Petrov, L., Fomalont, E.B., Gordon, D. 2007, AJ, 133, 1236
Kraus, A., Krichbaum, T.P., Wegner, R., et al. 2003, A&A, 401, 161
Labiano, A., Barthel, P.D., O'Dea, C.P., et al. 2007, A&A, 463, 97
Langston G.I., Heflin M.B., Conner S.R. et al. 1990, ApJS, 72, 621 (MITG)
Marecki, A., Falcke, H., Niezgoda, J., Garrington, S.T., & Patnaik, A.R. 1999, A&AS, 135, 273
Mutel, R.L. & Phillips, R.B. 1988, Proceedings of the 129th IAU Symposium, 129, 73
Ochsenbein, F., Bauer, P., Marcout, J. 2000, A&A, 143, 23
O'Dea, C.P. 1998, PASP, 110, 493
O'Dea, C.P. & Baum, S.A. 1997, AJ, 113, 148
Orienti, M., Dallacasa, D., Tinti, S., Stanghellini, C. 2006, A&A, 450, 959
Ott, M., Witzel, A., Quirrenbach, A., et al. 1994, A&A, 284, 331
Peck, A.B., & Taylor, G.B. 2000, ApJ, 534, 90
Petrov, L., Kovalev, Y.Y., Fomalont, E., Gordon, D. 2005, AJ, 129, 1163
Petrov, L., Kovalev, Y.Y., Fomalont, E.B., Gordon, D. 2006, AJ, 131, 1872
Petrov, L., Kovalev, Y.Y., Fomalont, E.B., Gordon, D. 2008, AJ, accepted; ArXiv e-prints 0801.3895
Readhead, A.C.S., Taylor, G.B., Pearson, T.J., Wilkinson, P.N. 1996, ApJ, 460, 634
Snellen I.A.G., Schilizzi, R.T., de Bruyn, A.G., et al. 1998, A&AS, 131, 435
Snellen, I.A.G., Schilizzi, R.T., & van Langevelde, H. J., 2000b, MNRAS, 319, 429
Snellen I.A.G., Schilizzi, R.T., Miley, G.K., et al. 2000a, MNRAS, 319, 445
Stanghellini, C., Bondi, M., Dallacasa, D., et al. 1997, A&A, 318, 376
Stanghellini, C., O'Dea, C.P., Dallacasa, D., et al. 1998, A&AS, 131, 303
Stanghellini, C., O'Dea, C. P., Dallacasa, D., et al. 2005, A&A, 443, 891
Torniainen, I., Tornikoski, M., Teräsranta H., et al. 2005, A&A, 435, 839
Véron-Cetty, M.-P. & Véron, P. 2006, A&A, 455, 773
Vollmer, B., Davoust, E., Dubois, P., et al. 2005a, A&A, 431, 1177
Vollmer, B., Davoust, E., Dubois, P., et al. 2005b, A&A, 436, 757
Wenger, M., Ochsenbein, F., Egret, D., et al. 2000, A&AS, 143, 9
Wright A.E., Griffith M.R., Burke B.F., & Ekers R.D. 1994, ApJS, 91, 111 (PMNS)
Wright A.E., Griffith M.R., Hunt A.J. et al. 1996, ApJS, 103, 145 (PMNZ)
Xiang, L., et al. 2002, A&A, 385, 768
Xiang, L., et al. 2005, A&A, 434, 123
Xiang, L., et al. 2006, A&A, 454, 729

Table 5. Results of the observations *The full table is available in electronic form at the CDS.*

Name (J2000)	RA, DEC (J2000)		Flux density (mJy)			Spectral index		Resolved
	(HHMMSS.ss)	(DDMMSS.s)	4.85 GHz	10.45 GHz	32.0 GHz	4.85/10.45 GHz	10.45/32.00 GHz	(GHz)
J0003+2129	000319.35	+212944.4	247 ± 2	173 ± 7	32 ± 3	−0.45 ± 0.05	−1.51 ± 0.09	
J0004+2019	000435.76	+201942.2	310 ± 2	382 ± 14	365 ± 19	0.27 ± 0.05	−0.03 ± 0.06	
J0005+5428	000504.37	+542824.9	448 ± 9	472 ± 3	413 ± 71	0.07 ± 0.03	−0.11 ± 0.15	
J0017+5312	001751.70	+531219.0	541 ± 11	518 ± 4	223 ± 38	−0.05 ± 0.03	−0.74 ± 0.15	
J0027+5958	002703.29	+595853.0	352 ± 2	370 ± 18	362 ± 34	0.06 ± 0.06	−0.01 ± 0.09	
J0037−2145	003714.79	−214524.5	235 ± 7	167 ± 4	139 ± 13	−0.43 ± 0.05	−0.16 ± 0.09	
J0048+0014	004819.10	+001457.0	87 ± 1	75 ± 3	51 ± 4	−0.18 ± 0.06	−0.35 ± 0.07	
J0057−0024	005717.00	−002433.0	198 ± 1	345 ± 17	296 ± 28	0.72 ± 0.06	−0.13 ± 0.09	
J0107+6521	010751.35	+652120.5	307 ± 2	294 ± 14	248 ± 23	−0.05 ± 0.06	−0.14 ± 0.09	
J0111+3906	011137.30	+390628.0	1315 ± 12	763 ± 32	207 ± 4	−0.70 ± 0.06	−1.16 ± 0.04	
J0113+6416	011350.58	+641651.6	41 ± 1	55 ± 3	51 ± 6	0.38 ± 0.08	−0.05 ± 0.11	
J0121+1127	012129.00	+112700.5	180 ± 1	141 ± 7	63 ± 7	−0.31 ± 0.07	−0.71 ± 0.11	
J0128+6306	012830.65	+630630.4	333 ± 2	452 ± 22	377 ± 35	0.40 ± 0.06	−0.15 ± 0.09	
J0201+6237	020153.26	+623757.3	80 ± 1	56 ± 2	−	−0.46 ± 0.04	−	10
J0203+1134	020346.60	+113445.0	976 ± 9	790 ± 4	490 ± 12	−0.27 ± 0.01	−0.42 ± 0.02	
J0219+4727	021923.33	+472740.0	278 ± 3	179 ± 2	99 ± 4	−0.56 ± 0.02	−0.52 ± 0.03	
J0247+5059	024758.36	+505907.1	80 ± 1	91 ± 2	82 ± 3	0.18 ± 0.03	−0.08 ± 0.04	
J0248+6214	024858.85	+621409.4	94 ± 1	67 ± 2	−	−0.44 ± 0.04	−	5
J0251+3734	025159.23	+373418.4	156 ± 2	154 ± 2	88 ± 3	−0.01 ± 0.02	−0.49 ± 0.03	
J0300+7359	030026.11	+735936.1	66 ± 2	45 ± 4	28 ± 8	−0.48 ± 0.13	−0.41 ± 0.28	
J0317+3306	031709.50	+330629.0	27 ± 1	17 ± 2	32 ± 7	−0.56 ± 0.14	0.56 ± 0.22	10/32
J0341+5217	034143.34	+521700.6	80 ± 2	73 ± 7	68 ± 19	−0.11 ± 0.13	−0.05 ± 0.26	
J0342+4809	034210.30	+480947.4	130 ± 5	116 ± 3	53 ± 20	−0.14 ± 0.06	−0.69 ± 0.35	
J0357+0542	035746.13	+054231.3	250 ± 4	196 ± 6	149 ± 12	−0.31 ± 0.05	−0.24 ± 0.08	
J0402−1458	040216.77	−145822.2	201 ± 3	138 ± 9	45 ± 4	−0.48 ± 0.08	−0.99 ± 0.09	
J0421+4352	042151.81	+435210.2	209 ± 8	152 ± 4	67 ± 25	−0.40 ± 0.06	−0.73 ± 0.34	
J0422+0219	042252.20	+021926.0	1471 ± 19	1273 ± 38	797 ± 62	−0.18 ± 0.04	−0.41 ± 0.07	
J0423−0120	042315.82	−012032.7	2396 ± 32	2617 ± 78	3638 ± 281	0.12 ± 0.04	0.29 ± 0.07	
J0424+0036	042446.80	+003607.0	1246 ± 17	1391 ± 42	1146 ± 89	0.14 ± 0.04	−0.16 ± 0.07	
J0428+3259	042805.80	+325951.0	521 ± 20	473 ± 9	160 ± 60	−0.12 ± 0.06	−0.96 ± 0.34	
J0434−1442	043419.00	−144255.0	256 ± 3	178 ± 11	91 ± 6	−0.46 ± 0.09	−0.59 ± 0.08	
J0437−1844	043701.40	−184448.0	935 ± 12	729 ± 45	314 ± 19	−0.31 ± 0.08	−0.74 ± 0.08	
J0445−1552	044511.54	−155213.1	57 ± 2	47 ± 3	30 ± 3	−0.25 ± 0.10	−0.38 ± 0.12	
J0446+3900	044611.49	+390017.1	331 ± 6	221 ± 13	109 ± 5	−0.52 ± 0.08	−0.62 ± 0.07	
J0504+4534	050431.35	+453416.0	40 ± 2	41 ± 6	−	0.03 ± 0.21	−	5/10
J0515+4152	051511.10	+415247.8	42 ± 1	41 ± 3	29 ± 3	−0.03 ± 0.10	−0.27 ± 0.12	32
J0529+3352	052951.69	+335218.2	57 ± 1	30 ± 6	−	−0.85 ± 0.26	−	5/10
J0530+1331	053056.40	+133155.0	3320 ± 19	3263 ± 16	2776 ± 389	−0.01 ± 0.01	−0.13 ± 0.13	
J0537+3947	053723.37	+394736.1	50 ± 1	27 ± 6	28 ± 6	−0.81 ± 0.27	0.04 ± 0.26	5/10/32
J0543+3023	054354.21	+302339.6	64 ± 1	61 ± 12	36 ± 5	−0.06 ± 0.25	−0.47 ± 0.22	
J0544+7132	054431.34	+713241.6	108 ± 2	71 ± 3	30 ± 3	−0.54 ± 0.05	−0.75 ± 0.09	
J0546+2422	054650.01	+242202.3	75 ± 1	78 ± 2	57 ± 3	0.06 ± 0.05	−0.28 ± 0.05	
J0549+3054	054954.16	+305447.7	76 ± 4	79 ± 10	65 ± 15	0.05 ± 0.18	−0.17 ± 0.23	
J0555+3330	055509.60	+333041.0	39 ± 2	26 ± 4	−	−0.49 ± 0.19	−	10
J0555+3948	055530.80	+394849.0	4986 ± 190	3660 ± 72	1242 ± 465	−0.39 ± 0.06	−0.96 ± 0.34	
J0601+3945	060118.21	+394550.7	128 ± 2	117 ± 2	74 ± 3	−0.11 ± 0.03	−0.40 ± 0.04	
J0601+1759	060155.36	+175948.6	121 ± 2	166 ± 3	121 ± 3	0.41 ± 0.03	−0.27 ± 0.03	
J0611+7218	061109.23	+721816.3	79 ± 2	80 ± 3	61 ± 3	0.01 ± 0.05	−0.24 ± 0.05	
J0623+3830	062328.94	+383049.8	290 ± 11	223 ± 5	49 ± 19	−0.33 ± 0.06	−1.35 ± 0.35	32
J0625+4440	062518.20	+444001.0	210 ± 2	215 ± 3	176 ± 4	0.03 ± 0.02	−0.17 ± 0.02	
J0626+8202	062602.90	+820225.0	690 ± 9	520 ± 11	352 ± 8	−0.36 ± 0.03	−0.34 ± 0.03	
J0632+3200	063230.79	+320053.7	137 ± 2	157 ± 2	91 ± 8	0.18 ± 0.03	−0.47 ± 0.08	
J0636+0801	063639.06	+080127.9	194 ± 4	128 ± 4	29 ± 2	−0.53 ± 0.05	−1.31 ± 0.08	32
J0637+1458	063751.06	+145857.9	230 ± 5	108 ± 3	26 ± 112	−0.98 ± 0.05	−1.25 ± 3.81	32
J0642+6758	064204.00	+675836.0	400 ± 5	301 ± 4	136 ± 19	−0.36 ± 0.02	−0.70 ± 0.13	
J0643−0108	064348.44	−010819.8	666 ± 5	627 ± 6	433 ± 8	−0.07 ± 0.02	−0.32 ± 0.02	
J0655+4100	065510.00	+410010.0	363 ± 6	393 ± 2	278 ± 23	0.10 ± 0.02	−0.30 ± 0.07	

Table 5. Results of the observations (continued)

Name (J2000)	RA, DEC (J2000)		Flux density (mJy)			Spectral index		Resolved
	(HHMMSS.ss)	(DDMMSS.s)	4.85 GHz	10.45 GHz	32.0 GHz	4.85/10.45 GHz	10.45/32.00 GHz	(GHz)
J0703 − 0517	070308.44	− 051717.5	128 ± 3	190 ± 5	135 ± 4	0.52 ± 0.04	−0.29 ± 0.03	
J0708 + 3524	070849.56	+ 352422.0	60 ± 2	52 ± 2	−	−0.18 ± 0.05	−	5
J0713 + 4349	071338.10	+ 434917.0	1543 ± 77	973 ± 119	398 ± 89	−0.59 ± 0.17	−0.79 ± 0.23	
J0717 − 1319	071711.52	− 131904.7	36 ± 2	26 ± 26	22 ± 19	−0.42 ± 1.31	−0.15 ± 1.19	10
J0717 + 5231	071729.99	+ 523104.9	124 ± 2	85 ± 2	43 ± 5	−0.49 ± 0.04	−0.59 ± 0.10	5
J0722 + 3722	072201.20	+ 372228.0	201 ± 10	154 ± 19	65 ± 15	−0.34 ± 0.17	−0.76 ± 0.23	
J0728 + 5907	072847.24	+ 590734.2	54 ± 2	52 ± 2	33 ± 4	−0.06 ± 0.05	−0.39 ± 0.11	
J0735 − 1324	073511.85	− 132400.4	51 ± 2	58 ± 2	63 ± 3	0.17 ± 0.06	0.06 ± 0.05	
J0740 + 2852	074033.50	+ 285247.0	146 ± 1	119 ± 23	66 ± 8	−0.26 ± 0.25	−0.51 ± 0.20	
J0745 − 0044	074554.00	− 004417.0	1899 ± 9	1519 ± 68	763 ± 162	−0.28 ± 0.06	−0.60 ± 0.19	
J0750 + 3040	075006.39	+ 304020.1	24 ± 2	35 ± 2	−	0.51 ± 0.13	−	5/10
J0811 + 4308	081137.38	+ 430829.3	162 ± 6	92 ± 3	−	−0.74 ± 0.06	−	
J0836 + 2728	083622.80	+ 272852.0	428 ± 16	433 ± 9	302 ± 50	0.02 ± 0.06	−0.31 ± 0.15	
J0847 − 2144	084759.73	− 214449.8	25 ± 1	−	−	−	−	5
J0854 + 2006	085448.8	+ 200630.0	2068 ± 9	3217 ± 144	3673 ± 779	0.58 ± 0.06	0.12 ± 0.19	
J0856 + 1739	085656.60	+ 173947.0	149 ± 3	136 ± 2	58 ± 5	−0.11 ± 0.03	−0.76 ± 0.08	
J0904 + 6934	090406.46	+ 693455.8	66 ± 3	52 ± 2	58 ± 10	−0.31 ± 0.08	0.10 ± 0.16	
J0907 + 4935	090756.34	+ 493548.2	38 ± 1	24 ± 2	26 ± 4	−0.55 ± 0.10	0.04 ± 0.14	5/10
J0930 + 7420	093053.70	+ 742005.0	305 ± 4	259 ± 4	161 ± 22	−0.20 ± 0.02	−0.42 ± 0.12	
J0943 − 1204	094323.52	− 120456.1	119 ± 3	57 ± 6	25 ± 10	−0.95 ± 0.13	−0.73 ± 0.38	32
J0948 + 5535	094832.02	+ 553535.1	27 ± 1	27 ± 2	33 ± 4	0.00 ± 0.10	0.18 ± 0.12	10
J0948 + 0022	094857.32	+ 002225.6	301 ± 4	394 ± 5	385 ± 33	0.35 ± 0.03	−0.01 ± 0.08	
J1008 + 0621	100800.82	+ 062121.2	474 ± 6	507 ± 7	482 ± 42	0.09 ± 0.02	−0.03 ± 0.08	
J1014 + 3813	101457.72	+ 381311.2	36 ± 1	32 ± 2	27 ± 3	−0.14 ± 0.08	−0.13 ± 0.12	
J1020 + 4320	102027.20	+ 432056.0	266 ± 2	180 ± 6	87 ± 4	−0.50 ± 0.04	−0.63 ± 0.05	
J1021 + 4114	102142.22	+ 411441.6	78 ± 2	94 ± 10	63 ± 7	0.24 ± 0.14	−0.35 ± 0.14	
J1022 + 3116	102230.59	+ 311629.8	13 ± 1	24 ± 3	−	0.86 ± 0.23	−	5/10
J1045 + 0624	104552.73	+ 062436.5	269 ± 2	257 ± 8	146 ± 3	−0.05 ± 0.04	−0.49 ± 0.04	
J1047 + 3945	104703.27	+ 394545.3	31 ± 1	20 ± 2	−	−0.57 ± 0.12	−	5/10
J1059 − 1134	105912.60	− 113422.0	256 ± 1	277 ± 13	333 ± 71	0.11 ± 0.06	0.16 ± 0.19	
J1106 + 6033	110656.68	+ 603359.6	36 ± 1	35 ± 2	37 ± 3	−0.05 ± 0.09	0.07 ± 0.08	5
J1108 + 0811	110837.50	+ 081101.6	177 ± 3	194 ± 21	146 ± 15	0.12 ± 0.14	−0.24 ± 0.13	
J1113 + 6853	111349.49	+ 685357.4	119 ± 1	100 ± 4	79 ± 3	−0.22 ± 0.05	−0.20 ± 0.05	
J1121 − 0711	112142.10	− 071106.0	309 ± 4	326 ± 35	−	0.07 ± 0.14	−	
J1135 + 3010	113514.09	+ 301005.7	94 ± 1	109 ± 3	133 ± 7	0.19 ± 0.04	0.17 ± 0.05	5
J1136 − 0330	113624.50	− 033029.0	480 ± 6	521 ± 56	365 ± 36	0.11 ± 0.14	−0.31 ± 0.13	
J1143 + 6619	114338.12	+ 661946.2	109 ± 3	74 ± 3	28 ± 3	−0.49 ± 0.07	−0.86 ± 0.11	
J1145 − 2250	114522.00	− 225031.0	372 ± 8	295 ± 27	320 ± 88	−0.29 ± 0.12	0.07 ± 0.26	
J1146 − 2447	114608.10	− 244732.0	1561 ± 32	1057 ± 98	533 ± 146	−0.50 ± 0.12	−0.60 ± 0.26	
J1200 + 4134	120019.08	+ 413416.3	34 ± 1	37 ± 2	39 ± 5	0.12 ± 0.09	0.04 ± 0.13	
J1208 + 0054	120833.68	+ 005422.0	235 ± 2	118 ± 5	40 ± 9	−0.89 ± 0.06	−0.95 ± 0.21	32
J1210 + 3552	121007.97	+ 355239.4	42 ± 1	45 ± 3	49 ± 13	0.10 ± 0.09	0.08 ± 0.24	10/32
J1212 − 2221	121203.65	− 222150.9	363 ± 5	406 ± 9	468 ± 10	0.15 ± 0.03	0.13 ± 0.03	
J1215 + 3250	121536.43	+ 325012.4	26 ± 1	17 ± 2	−	−0.50 ± 0.20	−	
J1219 + 6344	121910.59	+ 634410.7	135 ± 1	186 ± 7	115 ± 7	0.41 ± 0.05	−0.42 ± 0.06	
J1219 + 6600	121935.88	+ 660031.6	134 ± 4	153 ± 8	184 ± 32	0.17 ± 0.07	0.17 ± 0.16	
J1228 + 3706	122847.50	+ 370612.0	207 ± 2	255 ± 6	255 ± 13	0.27 ± 0.03	0.00 ± 0.05	5
J1235 − 1856	123543.56	− 185641.4	11 ± 16	−	−	−	−	
J1238 − 1743	123809.10	− 174344.2	55 ± 2	42 ± 2	43 ± 5	−0.33 ± 0.07	0.02 ± 0.11	
J1255 + 6527	125501.29	+ 652738.3	53 ± 2	31 ± 2	31 ± 7	−0.67 ± 0.10	0.00 ± 0.20	10/32
J1303 − 1051	130313.89	− 105116.7	357 ± 9	237 ± 3	55 ± 6	−0.52 ± 0.04	−1.30 ± 0.10	
J1310 + 3233	131059.40	+ 323334.0	715 ± 4	757 ± 17	838 ± 41	0.08 ± 0.03	0.09 ± 0.05	
J1311 + 5131	131113.52	+ 513138.6	26 ± 2	16 ± 2	−	−0.61 ± 0.16	−	5/10
J1322 + 3912	132255.66	+ 391208.0	197 ± 1	138 ± 3	63 ± 5	−0.45 ± 0.03	−0.69 ± 0.08	
J1341 + 2816	134115.28	+ 281605.1	241 ± 2	259 ± 6	224 ± 11	0.09 ± 0.03	−0.12 ± 0.05	
J1343 − 1747	134337.40	− 174756.0	618 ± 15	441 ± 4	343 ± 36	−0.43 ± 0.03	−0.22 ± 0.09	
J1353 + 7532	135323.16	+ 753257.7	419 ± 5	511 ± 4	282 ± 24	0.26 ± 0.02	−0.52 ± 0.08	

Table 5. Results of the observations (continued)

Name (J2000)	RA, DEC (J2000)		Flux density (mJy)			Spectral index		Resolved
	(HHMMSS.ss)	(DDMMSS.s)	4.85 GHz	10.45 GHz	32.0 GHz	4.85/10.45 GHz	10.45/32.00 GHz	(GHz)
J1359 + 5544	135905.75	+ 554429.3	84 ± 2	100 ± 2	142 ± 12	0.22 ± 0.04	0.31 ± 0.08	
J1359 + 4011	135938.09	+ 401138.3	314 ± 6	347 ± 42	258 ± 106	0.13 ± 0.16	−0.25 ± 0.38	
J1407 + 2827	140700.30	+ 282714.0	2572 ± 47	1469 ± 179	234 ± 96	−0.72 ± 0.16	−1.63 ± 0.38	
J1408 − 1529	140836.08	− 152924.4	50 ± 2	46 ± 2	43 ± 8	−0.10 ± 0.09	−0.03 ± 0.17	5
J1410 + 0731	141035.08	+ 073121.5	185 ± 4	198 ± 24	174 ± 72	0.09 ± 0.16	−0.10 ± 0.38	
J1420 + 1703	142020.89	+ 170329.2	276 ± 5	445 ± 54	423 ± 174	0.62 ± 0.16	−0.04 ± 0.38	
J1421 + 4645	142123.08	+ 464548.0	243 ± 5	229 ± 28	188 ± 77	−0.07 ± 0.16	−0.17 ± 0.38	
J1428 + 2724	142831.76	+ 272432.2	37 ± 1	58 ± 7	56 ± 23	0.58 ± 0.17	−0.01 ± 0.39	5
J1430 + 1043	143009.70	+ 104326.0	836 ± 15	628 ± 77	340 ± 140	−0.36 ± 0.16	−0.54 ± 0.38	
J1439 + 2114	143908.90	+ 211450.8	156 ± 3	169 ± 21	130 ± 53	0.10 ± 0.16	−0.22 ± 0.38	
J1439 + 1117	143912.04	+ 111740.6	41 ± 2	21 ± 3	−	−0.84 ± 0.20	−	5/10
J1452 + 5142	145202.08	+ 514252.6	46 ± 1	17 ± 2	−	−1.28 ± 0.19	−	10
J1458 + 3720	145844.80	+ 372021.0	220 ± 4	210 ± 26	186 ± 77	−0.05 ± 0.16	−0.10 ± 0.38	
J1511 + 5905	151157.92	+ 590504.7	46 ± 1	36 ± 3	45 ± 9	−0.32 ± 0.11	0.20 ± 0.19	5/32
J1521 + 4336	152149.61	+ 433639.3	256 ± 2	203 ± 9	173 ± 84	−0.29 ± 0.06	−0.13 ± 0.44	
J1530 + 5137	153019.78	+ 513730.2	76 ± 1	92 ± 5	115 ± 10	0.25 ± 0.07	0.20 ± 0.09	5
J1535 + 4957	153552.00	+ 495739.0	365 ± 2	300 ± 15	169 ± 14	−0.25 ± 0.07	−0.50 ± 0.09	
J1551 + 5806	155158.20	+ 580644.0	299 ± 2	342 ± 17	257 ± 21	0.18 ± 0.07	−0.25 ± 0.09	
J1603 + 1554	160338.06	+ 155402.4	358 ± 2	411 ± 17	258 ± 125	0.18 ± 0.05	−0.41 ± 0.44	
J1605 + 3038	160523.70	+ 303837.1	70 ± 2	54 ± 3	33 ± 79	−0.33 ± 0.08	−0.44 ± 2.16	5/10
J1612 − 1133	161214.82	− 113309.0	65 ± 2	58 ± 2	53 ± 5	−0.14 ± 0.07	−0.07 ± 0.10	
J1646 + 0042	164606.97	+ 004227.3	80 ± 3	121 ± 4	90 ± 8	0.53 ± 0.07	−0.25 ± 0.09	
J1658 + 5217	165834.62	+ 521729.2	57 ± 1	72 ± 3	−	0.30 ± 0.07	−	
J1714 − 2053	171432.46	− 205354.5	122 ± 4	99 ± 4	136 ± 20	−0.26 ± 0.06	0.28 ± 0.14	32
J1719 + 0817	171952.21	+ 081703.5	580 ± 3	419 ± 17	132 ± 64	−0.42 ± 0.05	−1.02 ± 0.44	
J1747 + 4658	174726.65	+ 465850.9	302 ± 7	336 ± 4	342 ± 36	0.14 ± 0.04	0.02 ± 0.09	
J1750 + 3231	175031.17	+ 323151.5	59 ± 1	58 ± 3	50 ± 25	−0.01 ± 0.07	−0.12 ± 0.44	5
J1750 − 1949	175042.51	− 194936.8	30 ± 2	29 ± 2	89 ± 9	−0.03 ± 0.13	1.00 ± 0.12	5/10
J1751 + 0939	175132.80	+ 093900.0	1590 ± 49	2168 ± 74	3098 ± 266	0.40 ± 0.06	0.32 ± 0.08	
J1752 + 7311	175211.62	+ 731120.2	160 ± 4	134 ± 7	133 ± 23	−0.22 ± 0.07	0.00 ± 0.16	
J1800 + 3848	180024.90	+ 384830.0	814 ± 11	1062 ± 151	1188 ± 52	0.35 ± 0.19	0.10 ± 0.13	
J1801 + 5751	180148.58	+ 575135.8	48 ± 1	39 ± 2	−	−0.26 ± 0.08	−	
J1810 − 1803	181056.14	− 180331.1	158 ± 2	−	−	−	−	5
J1823 + 7938	182314.11	+ 793849.0	623 ± 15	489 ± 25	176 ± 31	−0.30 ± 0.07	−0.90 ± 0.16	
J1828 − 1014	182801.34	− 101410.1	138 ± 2	145 ± 2	114 ± 10	0.06 ± 0.03	−0.21 ± 0.08	
J1834 − 0204	183426.41	− 020457.0	55 ± 1	21 ± 3	−	−1.23 ± 0.16	−	10
J1835 + 2506	183558.38	+ 250645.4	106 ± 2	43 ± 6	14 ± 45	−1.17 ± 0.19	−1.01 ± 2.99	32
J1843 − 0328	184356.93	− 032817.9	323 ± 5	117 ± 10	−	−1.31 ± 0.12	−	5/10
J1848 + 0138	184821.89	+ 013826.9	64 ± 2	105 ± 15	73 ± 4	0.64 ± 0.19	−0.32 ± 0.14	
J1850 + 2825	185027.59	+ 282513.1	1052 ± 15	1563 ± 222	999 ± 44	0.52 ± 0.19	−0.39 ± 0.13	
J1905 + 0601	190524.19	+ 060125.8	410 ± 8	365 ± 52	375 ± 17	−0.14 ± 0.19	0.02 ± 0.13	
J1917 + 1405	191718.11	+ 140509.2	111 ± 2	93 ± 13	76 ± 4	−0.22 ± 0.19	−0.17 ± 0.14	
J1922 + 2315	192212.27	+ 231521.4	29 ± 1	21 ± 2	31 ± 6	−0.38 ± 0.12	0.35 ± 0.19	10
J1926 + 1913	192613.84	+ 191359.0	59 ± 2	31 ± 4	−	−0.82 ± 0.19	−	5/10
J1927 + 1630	192733.97	+ 163001.2	194 ± 3	90 ± 3	20 ± 4	−0.99 ± 0.05	−1.34 ± 0.18	5/10
J1927 + 1623	192747.49	+ 162334.5	148 ± 2	39 ± 19	−	−1.73 ± 0.65	−	5/10
J1929 + 2325	192904.59	+ 232529.5	377 ± 5	190 ± 3	40 ± 6	−0.88 ± 0.03	−1.38 ± 0.14	
J1936 + 1942	193626.95	+ 194224.6	205 ± 3	210 ± 3	216 ± 30	0.03 ± 0.03	0.02 ± 0.12	
J1936 + 2051	193648.01	+ 205137.4	71 ± 2	69 ± 2	35 ± 6	−0.04 ± 0.06	−0.59 ± 0.14	
J1945 + 2120	194522.32	+ 212002.8	63 ± 2	61 ± 30	73 ± 3	−0.03 ± 0.65	0.16 ± 0.44	5
J1946 + 2029	194645.82	+ 202925.2	105 ± 2	90 ± 2	67 ± 10	−0.19 ± 0.04	−0.25 ± 0.13	5
J1958 + 2438	195800.39	+ 243802.6	28 ± 1	17 ± 9	16 ± 9	−0.63 ± 0.67	−0.04 ± 0.66	5
J2000 + 3227	200042.08	+ 322741.4	28 ± 3	19 ± 2	−	−0.53 ± 0.19	−	10
J2002 + 4725	200210.40	+ 472528.0	734 ± 17	589 ± 11	368 ± 62	−0.28 ± 0.04	−0.41 ± 0.15	
J2002 + 4506	200252.09	+ 450608.3	281 ± 6	404 ± 8	497 ± 84	0.47 ± 0.04	0.19 ± 0.15	
J2006 + 6424	200617.69	+ 642445.4	250 ± 2	243 ± 10	314 ± 7	−0.03 ± 0.06	0.23 ± 0.04	
J2007 + 4029	200745.00	+ 402948.0	2718 ± 61	2166 ± 41	1933 ± 326	−0.29 ± 0.04	−0.09 ± 0.15	

Table 5. Results of the observations (continued)

Name (J2000)	RA, DEC (J2000)		Flux density (mJy)			Spectral index		Resolved
	(HHMMSS.ss)	(DDMMSS.s)	4.85 GHz	10.45 GHz	32.0 GHz	4.85/10.45 GHz	10.45/32.00 GHz	(GHz)
J2016 + 6450	201640.66	+ 645028.1	250 ± 4	245 ± 14	206 ± 7	−0.01 ± 0.08	−0.15 ± 0.06	
J2018 − 1109	201827.99	− 110955.1	363 ± 18	216 ± 5	–	−0.67 ± 0.07	–	
J2022 + 6136	202206.68	+ 613658.8	3034 ± 28	2714 ± 115	1347 ± 23	−0.14 ± 0.06	−0.62 ± 0.04	
J2022 + 3519	202235.65	+ 351936.8	44 ± 2	25 ± 2	27 ± 5	−0.72 ± 0.10	0.08 ± 0.18	5/10
J2026 + 3903	202611.61	+ 390332.8	116 ± 3	92 ± 2	51 ± 9	−0.30 ± 0.05	−0.52 ± 0.16	32
J2032 − 2125	203254.29	− 212516.6	91 ± 5	23 ± 2	–	−1.75 ± 0.11	–	
J2049 + 1003	204945.87	+ 100314.4	601 ± 12	577 ± 285	577 ± 12	−0.04 ± 0.65	0.00 ± 0.44	
J2051 + 4417	205155.47	+ 441722.6	385 ± 5	257 ± 21	79 ± 3	−0.51 ± 0.11	−1.05 ± 0.08	
J2058 + 5012	205815.15	+ 501253.7	23 ± 3	–	–	–	–	5
J2102 + 4702	210217.10	+ 470216.9	175 ± 3	239 ± 19	267 ± 7	0.40 ± 0.11	0.10 ± 0.08	
J2104 − 1121	210410.82	− 112148.5	683 ± 34	603 ± 13	438 ± 29	−0.15 ± 0.07	−0.28 ± 0.06	
J2107 + 4214	210701.76	+ 421409.9	5510 ± 74	5908 ± 480	5338 ± 126	0.09 ± 0.11	−0.08 ± 0.08	
J2114 + 1714	211440.64	+ 171422.4	154 ± 4	133 ± 2	–	−0.18 ± 0.04	–	
J2116 + 0225	211650.79	+ 022547.0	136 ± 3	58 ± 2	–	−1.11 ± 0.05	–	5
J2120 + 5153	212044.84	+ 515327.5	894 ± 13	1001 ± 81	886 ± 21	0.15 ± 0.11	−0.10 ± 0.08	
J2123 + 0535	212344.50	+ 053523.0	3325 ± 74	2848 ± 44	1892 ± 223	−0.19 ± 0.04	−0.36 ± 0.11	
J2128 + 5728	212853.57	+ 572817.9	13 ± 1	15 ± 2	–	0.16 ± 0.21	–	5
J2129 − 1538	212912.10	− 153842.0	1354 ± 17	1439 ± 10	652 ± 55	0.08 ± 0.02	−0.70 ± 0.08	
J2130 + 3332	213029.60	+ 333249.3	121 ± 3	72 ± 2	21 ± 8	−0.67 ± 0.05	−1.09 ± 0.32	32
J2131 + 5233	213150.22	+ 523351.0	116 ± 2	113 ± 9	98 ± 3	−0.02 ± 0.11	−0.12 ± 0.08	
J2132 + 6316	213251.38	+ 631628.2	166 ± 2	180 ± 15	118 ± 4	0.11 ± 0.11	−0.37 ± 0.08	
J2136 + 0041	213638.70	+ 004155.0	10058 ± 143	7655 ± 213	3613 ± 331	−0.35 ± 0.04	−0.66 ± 0.09	
J2138 + 4318	213819.57	+ 431820.8	72 ± 2	50 ± 2	–	−0.46 ± 0.06	–	
J2140 − 1923	214046.85	− 192356.2	138 ± 2	128 ± 2	102 ± 9	−0.09 ± 0.03	−0.19 ± 0.08	
J2144 + 3453	214459.53	+ 345344.9	56 ± 2	28 ± 3	–	−0.88 ± 0.15	–	5
J2145 + 7114	214527.83	+ 711456.2	44 ± 2	43 ± 3	29 ± 3	−0.02 ± 0.10	−0.37 ± 0.11	5/10
J2151 + 0552	215137.80	+ 055212.0	845 ± 13	611 ± 11	312 ± 38	−0.41 ± 0.03	−0.59 ± 0.11	
J2156 − 0037	215614.70	− 003705.0	199 ± 3	–	309 ± 28	–	–	
J2204 + 3632	220421.10	+ 363237.1	220 ± 3	211 ± 4	137 ± 17	−0.04 ± 0.03	−0.38 ± 0.11	
J2208 + 6132	220812.13	+ 613256.0	78 ± 2	46 ± 2	26 ± 4	−0.70 ± 0.06	−0.48 ± 0.14	5/32
J2231 + 5922	223117.20	+ 592200.9	997 ± 14	953 ± 22	509 ± 47	−0.05 ± 0.04	−0.55 ± 0.08	
J2233 + 3339	223305.40	+ 333958.0	51 ± 2	37 ± 2	32 ± 5	−0.40 ± 0.07	−0.13 ± 0.14	5
J2236 + 2828	223622.40	+ 282855.0	740 ± 4	686 ± 26	755 ± 38	−0.09 ± 0.05	0.08 ± 0.06	
J2237 − 2506	223718.32	− 250632.9	300 ± 4	126 ± 2	18 ± 8	−1.12 ± 0.03	−1.73 ± 0.39	
J2245 + 0324	224528.28	+ 032408.9	483 ± 3	418 ± 16	278 ± 14	−0.18 ± 0.05	−0.36 ± 0.06	
J2249 + 5954	224929.13	+ 595456.3	2195 ± 19	1603 ± 67	714 ± 12	−0.40 ± 0.06	−0.71 ± 0.04	32
J2252 − 2042	225228.68	− 204732.2	171 ± 2	123 ± 2	41 ± 7	−0.42 ± 0.03	−0.97 ± 0.16	
J2258 + 4937	225825.27	+ 493744.6	38 ± 2	38 ± 2	39 ± 8	−0.01 ± 0.09	0.03 ± 0.18	5
J2302 + 5149	230247.14	+ 514916.0	54 ± 2	43 ± 2	34 ± 19	−0.31 ± 0.08	−0.19 ± 0.51	10
J2307 − 2247	230738.60	− 224753.0	666 ± 13	505 ± 4	366 ± 63	−0.35 ± 0.03	−0.28 ± 0.15	
J2343 + 6626	234326.78	+ 662607.2	108 ± 3	55 ± 2	50 ± 11	−0.87 ± 0.06	−0.07 ± 0.21	
J2355 − 2125	235502.10	− 212537.1	517 ± 11	277 ± 2	77 ± 14	−0.80 ± 0.03	−1.13 ± 0.16	
J2358 − 1020	235810.80	− 102008.0	883 ± 18	982 ± 7	1014 ± 174	0.14 ± 0.03	0.03 ± 0.15	

Table 6. Properties of the sources. *The full table is available in electronic form at the CDS.*

Name (J2000)	redshift	VCS	type	GPS/HFP	sample	var./ext.	$\nu_{\rm peak}$ (MHz)	$S_{\rm peak}$ (mJy)	note	$c_{8.6\rm GHz}$	$c_{2.3\rm GHz}$	class.
J0003 + 2129	0.450	y	Sy2	HFP	DL		6800	246		0.71	0.64	cso
J0004 + 2019	0.677	y	BLL			V				0.25	0.92	nc
J0005 + 5428		y							low b	0.71	0.89	nc
J0017 + 5312		y		GPS	M		2900	721	low b	0.26	0.28	cj/cso
J0027 + 5958		y				V			low b	0.86	< 0.72	nc
J0037 − 2145		y	rG							0.45	0.75	cj
J0048 + 0014	1.536		QSO									
J0057 − 0024	2.795	y	QSO							0.96	1.07	nc
J0107 + 6521			HII						low b			
J0111 + 3906		y	rG	GPS	DSL		4900	1292		0.12	0.16	cso
J0113 + 6416						V			low b			
J0121 + 1127		y		HFP			5700	185		0.77		nc
J0128 + 6306		y	G						low b			
J0201 + 6237				HFP		E	5500	77	low b			
J0203 + 1134	3.61	y	QSO	GPS	L		3700	984		0.71	0.81	cj
J0219 + 4727		y		GPS			4300	194		0.37	0.61	nc
J0247 + 5059			X						low b			
J0248 + 6214				GPS		E	3400	110	low b			
J0251 + 3734				HFP			9800	150				
J0300 + 7359				GPS			4900	56				
J0317 + 3306						EV						
J0341 + 5217									low b			
J0342 + 4809		y		GPS		V	4900	132	low b	< 0.48	0.55	cj
J0357 + 0542		y	QSO							0.48	0.26	nc
J0402 − 1458		y		HFP			6100	183		< 0.40	0.58	cj
J0421 + 4352		y		GPS			4300	199	low b	< 0.36	0.64	nc
J0422 + 0219	2.278	y	QSO	HFP			5600	1103		0.58	0.86	cj
J0423 − 0120	0.915	y	Bla			V				0.66	0.78	cj
J0424 + 0036		y	BLL							0.85	0.77	nc
J0428 + 3259		y	G	HFP	D		12500	287		0.27	0.83	cj
J0434 − 1442	1.899	y	QSO	GPS			3500	247		0.69	0.88	cj
J0437 − 1844	2.702	y	QSO	GPS	L		3500	1050		0.42	0.71	cj
J0445 − 1552			GiC			V						
J0446 + 3900		y		HFP			6800	248	low b	0.68	0.86	cj
J0504 + 4534						EV			low b			
J0515 + 4152				GPS		EV	2700	41	low b			
J0529 + 3352						EV			low b			
J0530 + 1331	2.07	y	QSO							0.51	0.44	cj
J0537 + 3947						E			low b			
J0543 + 3023									low b			
J0544 + 7132				HFP	B		6200	70				
J0546 + 2422				GPS			4700	77	low b			
J0549 + 3054		y				V			low b	< 0.80	< 0.71	nc
J0555 + 3330						EV			low b			
J0555 + 3948	2.363	y	QSO	HFP			6300	4537	low b	0.40	0.67	cj
J0601 + 3945				HFP			7400	96	low b			
J0601 + 1759				HFP			8100	125	low b			
J0611 + 7218					B							
J0623 + 3830		y		HFP		E	8100	203		0.72	0.69	nc
J0625 + 4440		y	BLL		DL					0.90	1.01	nc
J0626 + 8202	0.71	y	QSO							0.46	0.81	cj
J0632 + 3200		y		HFP			11000	154		0.91	< 0.81	nc
J0636 + 0801			∗iC	HFP		E	6800	168	low b			
J0637 + 1458		y				EV			low b	0.49	0.41	cj
J0642 + 6758	3.177	y	QSO	GPS	DL		4800	399		0.39	0.85	nc
J0643 − 0108			G	GPS			2600	700	low b			
J0655 + 4100		y	rG	HFP	DM		5900	384		0.64	0.88	nc

Table 6. Properties of the sources (continued)

Name (J2000)	redshift	VCS	type	GPS/HFP	sample	var./ext.	$\nu_{\rm peak}$ (MHz)	$S_{\rm peak}$ (mJy)	note	$c_{8.6\rm GHz}$	$c_{2.3\rm GHz}$	class.
J0703 − 0517				HFP			8700	142	low b			
J0708 + 3524						E						
J0713 + 4349	0.518	y	EmG	GPS	SL		2100	2233		0.14	0.35	cso
J0717 − 1319						EV			low b			
J0717 + 5231				GPS		E	3400	130				
J0722 + 3722	1.629	y	QSO	GPS	DM	V	4200	223		0.33	0.91	cj
J0728 + 5907				HFP			8700	50				
J0735 − 1324						V			low b			
J0740 + 2852	0.711	y	QSO	HFP			5500	132		0.98	1.05	nc
J0745 − 0044	0.994	y	QSO	HFP	SL		13300	1045		0.12	0.71	cj
J0750 + 3040						EV						
J0811 + 4308				GPS			1300	267				
J0836 + 2728	0.765	y	QSO							0.40	0.65	cj
J0847 − 2144						EV						
J0854 + 2006	0.306	y	QSO			V				0.52	0.79	cj
J0856 + 1739				HFP			6100	159				
J0904 + 6934												
J0907 + 4935			PaG			E						
J0930 + 7420		y		GPS	M		4500	290		0.29	0.51	cj
J0943 − 1204		y				EV						nc
J0948 + 5535						E						
J0948 + 0022	0.584	y	Sy1							0.87		nc
J1008 + 0621		y	X							0.67	0.97	nc
J1014 + 3813	1.927		QSO			V						
J1020 + 4320	1.96	y	QSO	HFP	M		7200	186		< 0.31	0.77	nc
J1021 + 4114			X			V						
J1022 + 3116						EV			ext?			
J1045 + 0624	1.507	y	QSO	HFP	D	V	5500	282		0.80	0.99	nc
J1047 + 3945						EV						
J1059 − 1134		y	BLL			V				0.72	0.98	nc
J1106 + 6033						E						
J1108 + 0811		y								0.99	< 0.63	nc
J1113 + 6853												
J1121 − 0711		y	BLL							0.80	0.75	cj
J1135 + 3010						E						
J1136 − 0330	1.648	y	QSO	HFP			9000	417		0.83	0.99	nc
J1143 + 6619				HFP			5300	105				
J1145 − 2250	1.141	y	QSO			V				0.48	0.34	cj
J1146 − 2447	1.940	y	QSO	HFP	SL		6800	1092		0.17	0.72	cj
J1200 + 4134						V						
J1208 + 0054		y		HFP		E	5800	205		< 0.49	0.51	cj
J1210 + 3552			G			E						
J1212 − 2221		y								0.37	0.85	cj
J1215 + 3250						V						
J1219 + 6344		y		HFP			11800	186		0.43		nc
J1219 + 6600	1.266	y	QSO							0.53	0.68	nc
J1228 + 3706	1.515	y	QSO			EV				0.82	0.89	cj
J1235 − 1856						V						
J1238 − 1743												
J1255 + 6527						E						
J1303 − 1051		y	BLL	GPS			4600	446		< 0.75	< 0.88	cj
J1310 + 3233	1.65	y	QSO							0.61	0.90	cj
J1311 + 5131				GPS		E	4900	26				
J1322 + 3912	2.982	y	QSO	HFP			6900	155		< 0.41	0.72	nc
J1341 + 2816	1.31	y	QSO							0.90	0.97	nc
J1343 − 1747	1.50	y	QSO							< 0.18	0.56	cj
J1353 + 7532		y		HFP			9400	384		0.80	0.98	nc

Table 6. Properties of the sources (continued)

Name (J2000)	redshift	VCS	type	GPS/HFP	sample	var./ext.	$\nu_{\rm peak}$ (MHz)	$S_{\rm peak}$ (mJy)	note	$c_{8.6\rm GHz}$	$c_{2.3\rm GHz}$	class.
J1359 + 5544		y				V					0.57	nc
J1359 + 4011	0.407	y	EmG		M					0.85	1.00	nc
J1407 + 2827	0.077	y	Sy1	HFP	DSL		5900	2550		0.42	0.48	cso
J1408 − 1529			X			EV						
J1410 + 0731		y				V				0.51	0.58	cj
J1420 + 1703		y								0.89		nc
J1421 + 4645	1.665	y	QSO							0.68	0.95	nc
J1428 + 2724	0.014		LIN			EV						
J1430 + 1043	1.71	y	QSO	HFP	DL		5200	682		0.29	0.95	nc
J1439 + 2114		y								0.65	< 0.69	cj
J1439 + 1117						EV						
J1452 + 5142	0.476		QSO			EV						
J1458 + 3720	0.333	y	QSO			V				0.57	0.65	cj
J1511 + 5905						E						
J1521 + 4336	2.18	y	QSO							0.86	0.94	cj
J1530 + 5137						E						
J1535 + 4957	1.119	y	QSO	HFP	M		6100	333		0.59	0.91	nc
J1551 + 5806	1.320	y	QSO		B					0.48	0.63	nc
J1603 + 1554	0.109	y	QSO	HFP			11500	308		0.96	0.75	nc
J1605 + 3038	2.67		QSO	GPS		E	4500	68				
J1612 − 1133						V						
J1646 + 0042		y	X							0.78		nc
J1658 + 5217												
J1714 − 2053		y				E				< 0.60	< 0.66	nc
J1719 + 0817		y		HFP			7800	425		0.49	0.67	cj
J1747 + 4658	> 1.484	y	BLL			V				0.74	0.77	cj
J1750 + 3231						E						
J1750 − 1949			IR			EV			low b			
J1751 + 0939	0.320	y	BLL	HFP	D		10500	2323		0.85	0.67	cj
J1752 + 7311		y								0.70	0.94	nc
J1800 + 3848	2.092	y	QSO		D					0.77	0.68	cj
J1801 + 5751			X			V						
J1810 − 1803						EV			low b			
J1823 + 7938	0.224	y	Sy2	HFP			9000	498		0.15	0.41	cso
J1828 − 1014			PN						low b			
J1834 − 0204						EV			low b			
J1835 + 2506	1.973		QSO	GPS		E	4500	103				
J1843 − 0328			IR			EV			low b			
J1848 + 0138						V			low b			
J1850 + 2825	2.56	y	QSO	HFP	DL		10600	1251		0.17	0.62	cj
J1905 + 0601			IR						low b			
J1917 + 1405			IR						low b			
J1922 + 2315						EV			low b			
J1926 + 1913			IR	GPS		E	4800	59	low b			
J1927 + 1630			IR			EV			low b			
J1927 + 1623			IR			EV			low b			
J1929 + 2325		y		GPS			4000	393	low b	0.31	0.40	nc
J1936 + 1942			PN						low b			
J1936 + 2051				HFP			7100	59	low b			
J1945 + 2120			PN			E			low b			
J1946 + 2029						E			low b			
J1958 + 2438				GPS		E	3900	30	low b			
J2000 + 3227			PN			EV			low b			
J2002 + 4725		y	X	GPS	M		3600	728	low b	0.82	0.92	nc
J2002 + 4506		y							low b	0.85	0.63	cj
J2006 + 6424	1.574	y	QSO		M	V				0.25	0.93	nc
J2007 + 4029	1.736	y	QSO						low b	< 0.03	0.09	cj

Table 6. Properties of the sources (continued)

Name (J2000)	redshift	VCS	type	GPS/HFP	sample	var./ext.	$\nu_{\rm peak}$ (MHz)	$S_{\rm peak}$ (mJy)	note	$c_{8.6\rm GHz}$	$c_{2.3\rm GHz}$	class.
J2016 + 6450												
J2018 − 1109		y		HFP			6500	249		0.44	0.92	cj
J2022 + 6136	0.227	y	Sy2	GPS			4900	3050		0.25	0.18	cso
J2022 + 3519						EV			low b			
J2026 + 3903			IR	HFP		E	5500	105	low b			
J2032 − 2125		y				V					0.88	nc
J2049 + 1003		y		HFP			6300	527		0.44	0.54	cj
J2051 + 4417				HFP			5800	346	low b			
J2058 + 5012						EV			low b			
J2102 + 4702		y		HFP			9600	227	low b	0.78		nc
J2104 − 1121			PN									
J2107 + 4214			PN						low b			
J2114 + 1714												
J2116 + 0225			G			EV						
J2120 + 5153			PN?						low b			
J2123 + 0535	1.941	y	QSO	HFP	D		15700	2161		0.25	0.77	cj
J2128 + 5728						EV			low b			
J2129 − 1538	3.28	y	QSO	HFP	SL		9400	1151		0.42	0.79	cj
J2130 + 3332	1.473		QSO	GPS		E	4800	133				
J2131 + 5233			PN						low b			
J2132 + 6316				HFP			13100	135	low b			
J2136 + 0041	1.932	y	QSO	HFP	DS		5300	8645		0.25	0.42	cj
J2138 + 4318				HFP			9000	58	low b			
J2140 − 1923		y								0.72	0.78	nc
J2144 + 3453				HFP		E	9300	40				
J2145 + 7114				GPS		E	3900	48				
J2151 + 0552	0.740	y	Sy1	GPS	L		3900	876		0.45	0.60	cj
J2156 − 0037	0.495	y	BLL			V				0.69	0.96	nc
J2204 + 3632		y	G	HFP			9300	222		< 0.43	0.95	nc
J2208 + 6132			*	GPS		E	3200	69	low b			
J2231 + 5922				HFP			10100	798	low b			
J2233 + 3339						E						
J2236 + 2828	0.795	y	QSO			V				0.64	0.93	cj
J2237 − 2506		y	G	GPS			2400	450			0.22	cj/cso
J2245 + 0324	1.34	y	QSO	HFP			6500	499		0.58	0.81	cj
J2249 + 5954			HII	GPS		E	4300	2268	low b			
J2252 − 2047		y		GPS			3400	160		< 0.43	0.48	nc
J2258 + 4937						EV			low b			
J2302 + 5149			X			E			low b			
J2307 − 2247		y		GPS			3900	500		0.34	0.14	cj/cso
J2343 + 6626				GPS			3600	119	low b			
J2355 − 2125		y		GPS			4500	508		< 0.33	0.49	cj
J2358 − 1020	1.622	y	QSO							0.78	0.89	cj

Col. (1): source name; col. (2): redshift from Véron-Cetty & Véron (2006); col. (3): VCS data 'y'= available; col. (4): object type from SIMBAD (rG: radio galaxy, IR: infrared source, GiC: galaxy in cluster; *iC: star in cluster, EmG: emisson line galaxy, PaG: Pair of galaxies, QSO: quasar, Sy: Seyfert galaxy, BLL: BL Lac-type object, X: X-ray source, PN: planetary nebula, *: star, G: galaxy, HII: HII region); col. (5): GPS/HFP, the classification criteria are described in Sect. 6; col. (6): sample membership (abbreviation as in Tab. 4); col. (7): 'V'=variable, 'E'=extended at 4.85 GHz; col. (8): peak frequency in MHz; col. (9): peak flux density in mJy; col. (10): low b=±10° from the Galactic plane, 'ext?'= source size > 45″; col. (11): compactness ratio at 8.6 GHz; col. (12): compactness ratio at 2.3 GHz; col. (13): classification based on VLBI images: 'nc'= naked core candidate; 'cj'= core-jet candidate; 'cso'= compact symmetric object candidate; 'cj/cso' = core-jet or compact symmetric object candidate, components cross-identification between 2 and 8 GHz is questionable; the VCS classification for the following sources was corrected according to deeper multi-frequency VLBI studies: J0003+2129 (Orienti et al. 2006), 1407+2827 (e.g., Stanghellini et al. 1997), J1551+5806 (Snellen et al. 2000); our cso candidates J0111+3906, J0713+4349, J1823+7938, J2022+6136 are confirmed by Peck & Taylor (2000).